Texas A&M University
Mechanical Engineering Department
Turbomachinery laboratory

Experimental force Coefficients for a Sealed Squeeze Film Damper: Test Rig Development

Research progress Report to the Turbomachinery Research Consortium

By

Adolfo Delgado

Research Assistant

Luis San Andrés

Professor

TRC-SFD-1-04
May 2004

TRC Project:
Experimental Force Coefficients for a Sealed Squeeze Film Damper (Phase I)

Executive Summary

High performance turbomachinery demands high shaft speeds, increased rotor flexibility, tighter clearances in flow passages, advanced materials, and increased tolerance to imbalances. Operation at high speeds induces severe dynamic loading with large amplitude journal motions at the bearing supports. At these conditions, squeeze film dampers (SFDs) with low levels of external pressurization are prone to air ingestion leading to an inhomogeneous lubricant film with large striations of entrapped gas. This pervasive phenomenon affects greatly the dynamic force capability of the support fluid film bearings and reduces the reliability of the rotor-bearing system.

The report details the design of a sealed SFD and the revamping of an existing test facility to accommodate the new mechanical element. The end sealed SFD replicates an industrial configuration with an annular discharge section with orifice ports and a wave spring and ring assembly pushing the journal. The test SFD will provide experimental results to assess the effect of the end seal on the damper forced performance. Structural parameters of the "dry" system (i.e. with no lubricant across the SFD land) were identified from static load and impact load tests.

Planned experiments and a methodology for the identification of the SFD parameters follow. Multi-frequency (sweep sine) and single frequency force excitation will make it possible to identify the SFD inertia and damping force coefficients. Two electromagnetic shakers were acquired to exert periodic forces of large magnitude (max. 100 lb) into the test SFD. The parameter identification method is a frequency domain procedure based on the Instrument Variable Method (IVF). The method anticipates the influence of "dry-friction" effects from contact surfaces (journal and push ring) in relative motion due to the assembly preload when fitting the wave spring.

Table of contents

List of Tables and Figures

Tables

Figures

List of Figures (continued)

Nomenclature

$a_{x,y}$ Bearing housing accelerations [m/s^2]

c bearing radial clearance [10 mils – design]

$C_{sx,sy}$ Dry (no lubricant) damping coefficients [N.s/m]

$C_{\alpha\beta}$ (Estimated) Bearing damping coefficients [N.s/m], $\alpha, \beta = X, Y$

C_{tt} Direct damping coefficient for circular centered orbits [N.s/m]

$D_{\alpha\beta}$ (Estimated) Bearing fluid inertia coefficients [N.s^2/m], $\alpha, \beta = X, Y$

D_{rr} Direct inertia coefficient for circular centered orbits [N.s^2/in],

$F_{x,y}$ External (shaker) forces applied to bearing [N]

$\overline{F}_{x,y}$ Frequency components of external forces applied to bearing [N]

f_n Natural frequency [Hz]

G Eddy current sensor gain

$H_{\alpha\alpha}$ Dynamic flexibility, $\alpha = X, Y$

i imaginary unit ($\sqrt{-1}$)

$K_{sx,sy}$ Structural (support) stiffnesses [N/m]

M Mass of bearing housing [kg]

M_f Estimated mass of lubricant (feed plenum and recirculation annulus) [kg]

T Lubricant temperature [°C]

U_α Experimental Uncertainty (α= measured variable)

X, Y Cartesian coordinate system for lateral motions of test bearing

x, y Bearing dynamic motions along two directions X, Y [m]

$\overline{x}, \overline{y}$ Frequency components of bearing motions [m]

$Z_{(\omega)}$ Displacement vector in the frequency domain [m]

ρ Lubricant density [kg/m^3]

μ Lubricant viscosity [Pa.s]

ω Excitation frequency [rad/s]

ω_n Natural frequency [rad/s]

ζ $C/[2\,(K_s M)^{1/2}]$. Viscous damping ratio

Introduction

Squeeze Film Dampers (SFDs) are still widely used to provide damping in aeroderivate gas turbines that are supported on rolling element bearings. SFDs aid to attenuate rotor synchronous responses at passage through critical speeds where shaft vibration amplitudes due to imbalance peaks. SFDs consist of a stationary journal (generally the outer race of a ball bearing) and a concentric housing separated by small gap filled with a lubricant. In operation, the dynamic motion of the journal (whirling) squeezes the thin lubricant film, thus generating hydrodynamic pressures and film forces able to dissipate mechanical energy [1].

SFD performance (damping capability) depends on its geometrical configuration as well as on its operational parameters such as flow regime, type of journal motion, lubricant cavitation and air entrapment among others [2]. In particular, the latter can lead to severe reduction of the damping coefficients [3,4]. Air entrapment occurs at sufficiently high whirl frequencies and large vibration amplitudes where air is ingested into the lubricant film, becoming entrapped, thus severely reducing the damper forced performance [5]. The severity of air ingestion and entrapment increases with frequency and journal amplitudes. This phenomenon is more pervasive in open ends SFD configurations, where at least one of the damper ends is exposed to ambient (air) pressure. Díaz and San Andrés [6, 7] present a study of the effects of air ingestion and entrapment in the forced response of an open end SFD.

Della Pietra and Adilleta [8] present an extensive review of the research conducted on SFDs in the past 40 years. The authors include a complete description of SFDs, their physical characteristics, predictive models and their correlation with numerous experimental results. In particular, the authors discuss different SFD end seal configurations.

Levesley and Holmes [9] compare the damping capacity an general performance of various SFD configurations, including different type of end seals. The results show that the end-sealed SFD provides more damping capacity and is less prone to the occurrence of vapor cavitation. The authors conclude that piston-ring sealed SFDs have a better performance over other two end seal arrangements tested (end-chambered end plates seals).

A sealed end SFD design and a description of the experimental facility for testing its rotordynamic performance follow. The SFD design is based upon a configuration used by one of the TRC sponsors. This is a first progress report of a continuation project whose ultimate objective is to identify the damping and inertia coefficient of the sealed SFD. The major tasks of the project are:

a) Conduct static and dynamic tests under "dry" conditions to determine the structure stiffness and test section natural frequencies. Develop identification technique and model to characterize end-seal friction (equivalent damping).
b) Measure pressure drop and leakage to determine the end seal coefficient as a function of pressure, lubricant temperature (viscosity), wave spring preload, journal centering, and orifice size.
c) Perform dynamic load tests (shakers) with lubricated SFD for increasing oil temperatures and feed pressures.
d) Develop test and DAQ procedures. Perform analysis of test data using frequency domain identification techniques to extract SFD force coefficients (damping and inertia). Forward estimated parameters as a function of excitation frequency and amplitude of whirl, lubricant flow rate, feed temperature and pressure, sealing conditions, etc.

Test rig description

The test rig comprises of a new acrylic bearing mounted on the same structure reported in previous TRC research projects [10]. Figure 1 shows a schematic view of the test rig structure accommodating the new bearing housing. A vertical rigid shaft mounted on three precision ball bearings (natural frequency 400 Hz [11]), holds a steel journal of 5"(127 mm) diameter and 3"(76.2 mm) long. The bearing assembly consists of the acrylic bearing sandwiched by two steel plates, attached by two vertical steel plates. These plates also serve as an interface to apply external forces onto the bearing assembly. The top plate includes a connection for lubricant supply through a flexible hose. A static pressure gauge displaying the feed pressure into the bearing and four eddy current sensors facing the shaft. The composite bearing housing hangs from a top structure with four steel rods giving a structural stiffness to the test bearing section.

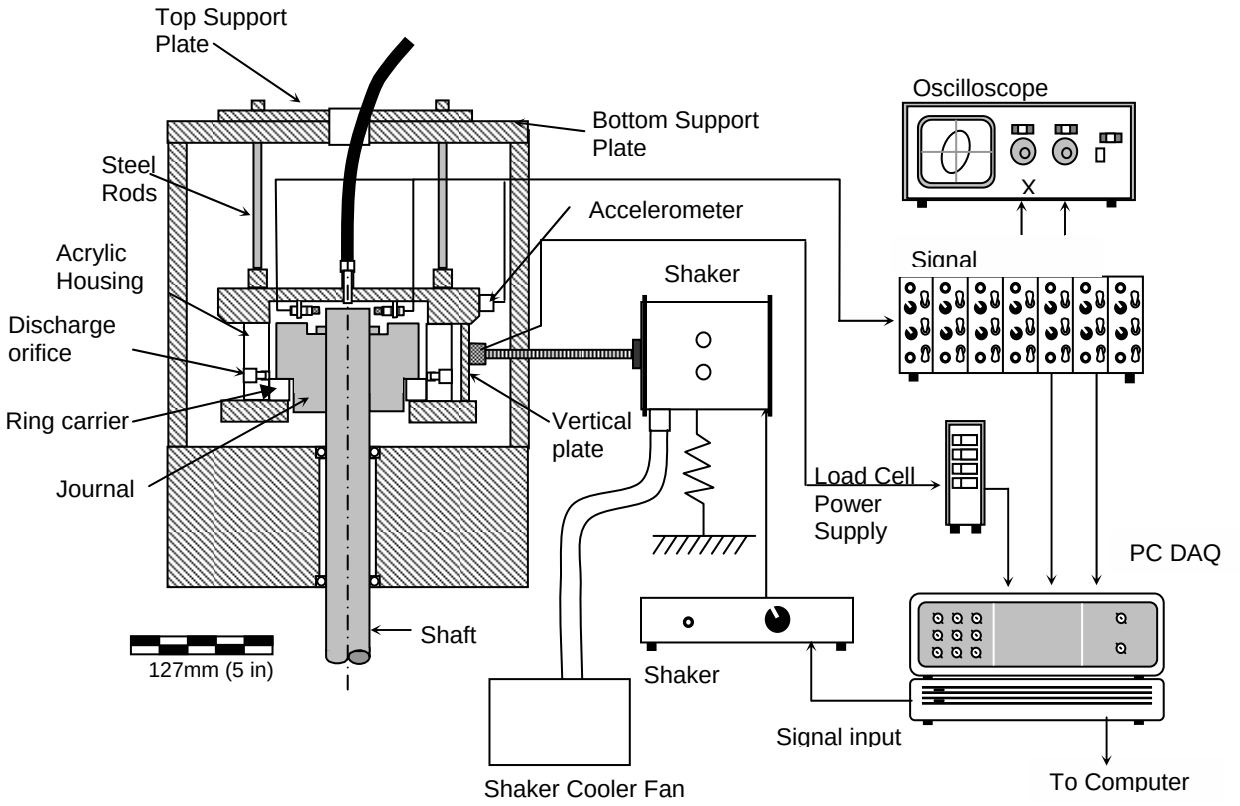

Figure 1 Test rig for dynamic force measurements and flow visualization in a sealed end SFD

A mechanism comprising two sliding flat plates (top and bottom support plates) on the top structure allows centering and off-centering positioning of the bearing with respect to the shaft [11].

Figure 2 shows the sensor disposition and reference coordinate system on the SFD housing. Two electromagnetic shakers (max. 100 lbf or 450 N), suspended from separate steel frames, stand to provide excitation forces onto the test device. Slender steel stingers connect the shaker to the bearing housing (*x* and *y* directions). Piezoelectric load cells are fastened to the side plates and the one of the stingers end. The top disk allocates two accelerometers *(x,y)*, right above the side plates.

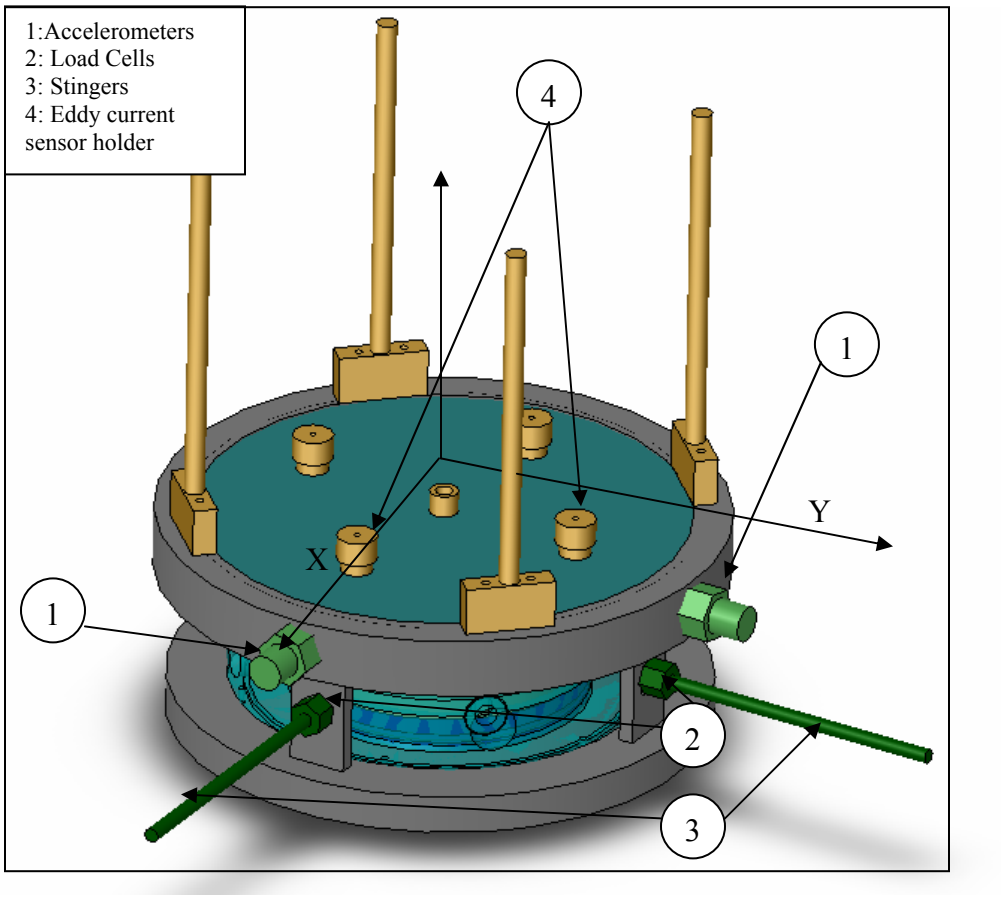

Figure 2 SFD housing reference coordinate system and location of sensors.

The new bearing housing design integrates a SFD land and an annulus that accommodates a metallic ring (ring holder). This metallic ring along with the journal bottom surface provides a metal-metal mechanical seal. A wave spring, pushing the ring holder against the journal, applies a contact force between the matting surfaces. Furthermore, different sets of shims make it possible to adjust the contact force between the surfaces. Figures 3 and 4 depict a cross section and a cut view of the new end sealed SFD design along with its components, respectively.

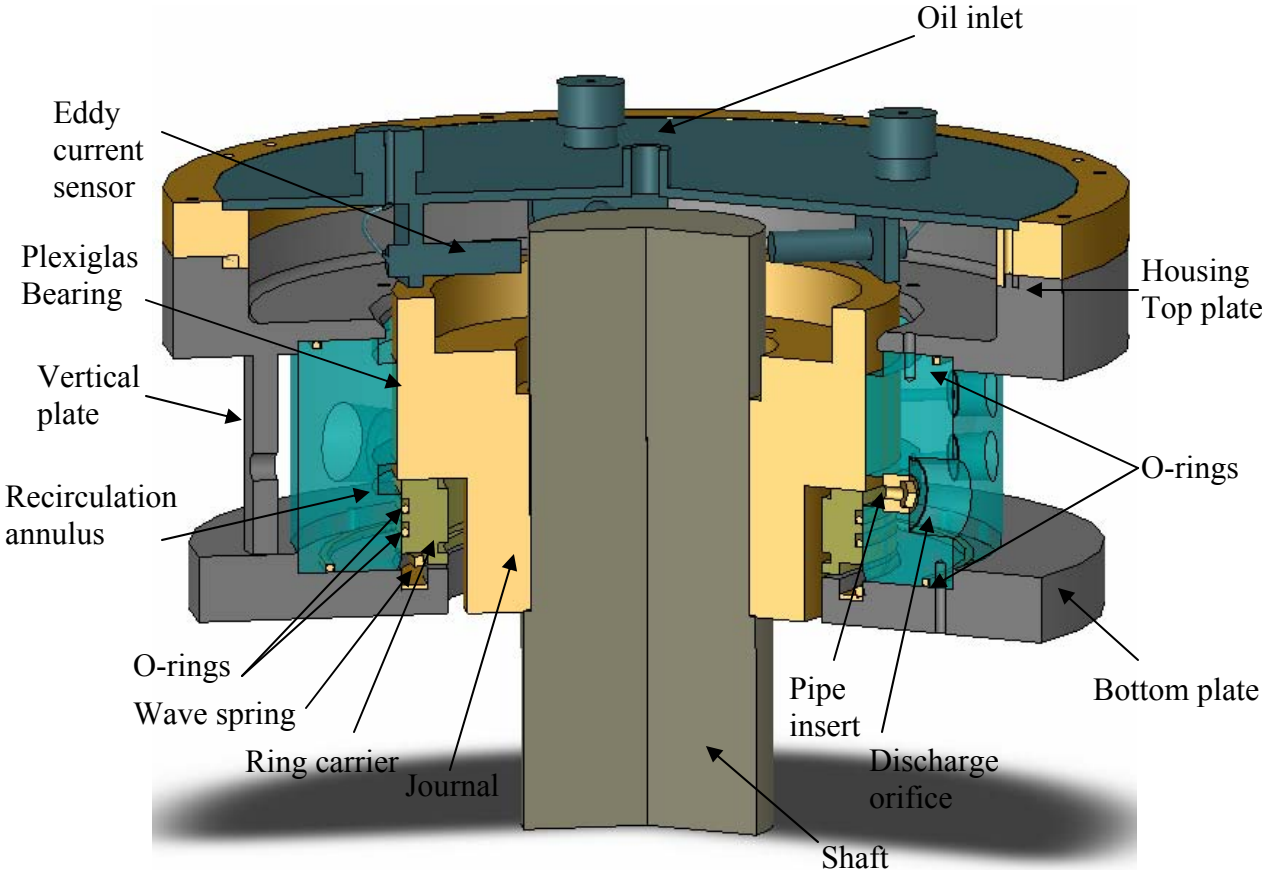

Figure 3 Sealed-end SFD assembly: cross section view

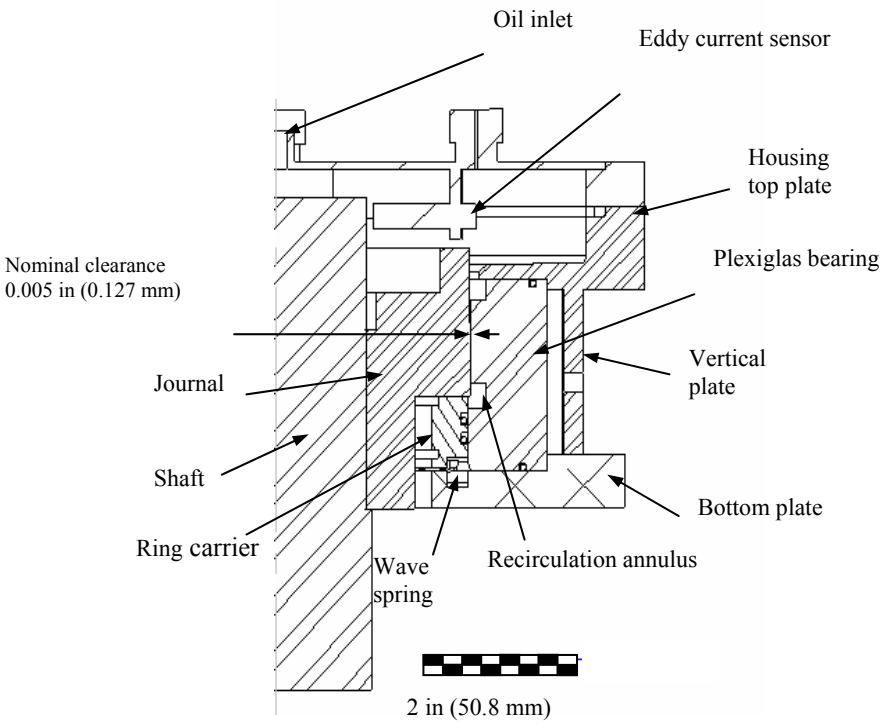

Figure 4 Sealed-end SFD assembly: cut view

The new SFD assembly incorporates the following main features:

- O-ring carrier with a 16 (μin) finish top surface, this component interacts with the journal to seal SFD at one side. Two O-rings mating the bearing inner diameter prevent leakage in between the two surfaces.
- Recirculation annulus to reduce oil starvation occurrence at the discharge end of the SFD land, i.e. close to the discharge ports and/or during negative strokes of the journal (i.e. when moving away from the bearing).
- Wave spring providing the normal force to enhance the mechanical seal conformed by the ring carrier and the journal bottom side. (maximum load, 100 lb)
- Four pipe inserts 3/8" set screws with a through hole to regulate the discharge flow.
- Four hose coupling allowing disconnecting a reconnecting the outlet hoses easily to replace pipe inserts with different orifice sizes.
- Two strain gauge pressure sensors and two thermocouples (T-type) facing the SFD land and recirculation annulus (180 degrees from positive Y axis. See Figure 2).

Lubrication system

Figure 5 depicts the lubrication system of the test rig, with the only difference between the previous and current system being the incorporation of two flowmeters and pipe lines for the four outlets of the new SFD configuration (end sealed). The flowmeters, located at the SFD inlet and outlet, will allow estimation of leakage flow through the SFD end seal.

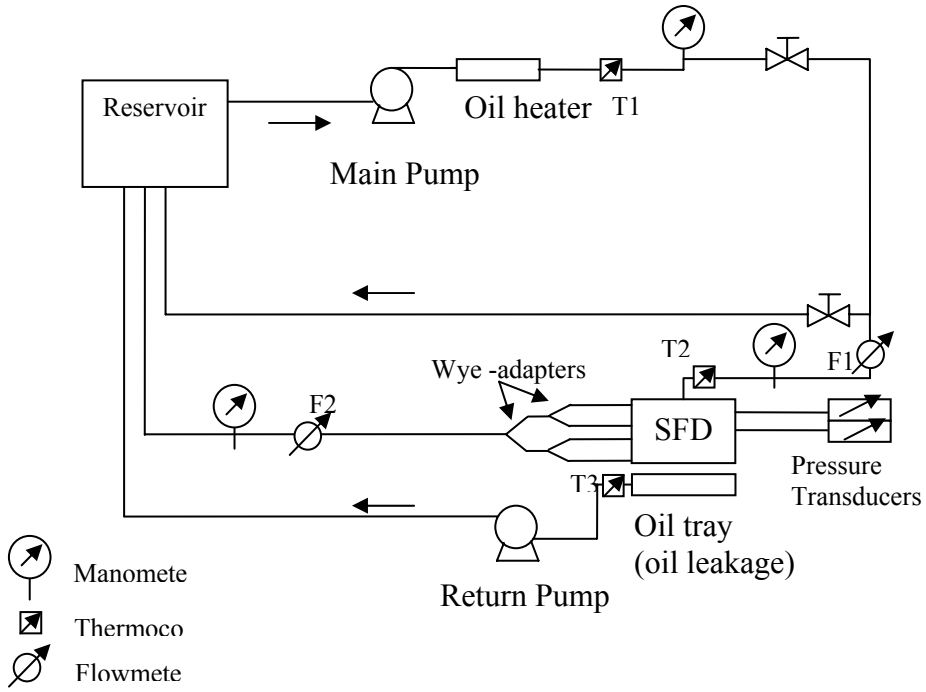

Figure 5 Schematic view of lubricant system.

The piping for connecting the SFD multiple oil outlets is symmetric in order to equalize the friction losses for each of the four outlets. This implies same longitude hoses and symmetric wye adapters.

The lubricant to be used is an ISO VG 2 with a density (ρ) of 736 kg/m^3 and its absolute viscosity follows is related to temperature (°C) by [12]:

$$\mu_{oil}(T) := 3.03 \cdot e^{-.0209 \cdot (T - 23.6)} \text{ cPoise} \quad (1)$$

Identification of test rig structural parameters

Static load and impact load tests performed on the SFD assembly allow the identification of the structural parameters (stiffness and damping) provided by the four steel rods that hold the SFD in position. The stiffness and damping coefficients, along with the SFD housing mass, provide the necessary information to characterize the SFD assembly parameters. These results will serve as a baseline for the experiments to be conducted with lubricant circulating through the SFD land.

Static tests

The diametral clearance of the SFD was determined by measuring the maximum deflection of the SFD assembly (SFD bearing + plates) while pushing it sideways back and forth in the *X* and *Y* direction. Table 1 shows the nominal[1] and measured diametral clearance in the *X* and *Y* direction. The measured clearance is within the design tolerance values (9.4 ±0.5 mils), yet it is expected to vary with temperature. Thus, clearance measurements will be performed before and following each test.

Table 1 SFD nominal and measured diametral clearance

	X	*Y*
Nominal [mils]	9.4 (0.239 mm)	9.4 (0.239 mm)
Measured [mils] @ 75 ^{0}F*	9.3 ± 0.4 (0.236 mm)	9.7 ±0.4 (0.246 mm)

*: Plexiglas housing temperature.

The weight of the SFD assembly was measured by suspending it from a force gauge as shown in Figure 6. The weight of the rods and blocks (connecting the rods to the SFD assembly) was measured using a scale (±0.001 lb). Table 2 shows the mass of each of the mentioned components and the estimated effective mass. Notice that for a steel rod, its effective mass is 1/3 of its total mass, since each rod is fixed as a cantilever beam.

Table 2 Measured weight and estimated effective mass of the SFD assembly and connecting rods.

	Weight [lb]
SFD Assembly [±0.5] *	25 (11.3 Kg)
Rods [±0.001]	1.3 (0.59 Kg)
Blocks[±0.001]	0.25 (0.11 Kg)
Total effective mass	25.7 (11.7) (±2%)

*: including hose connectors, ring carrier and sensors.

[1] The steel journal was hard chrome platted to increase O.D and attain the current nominal clearance for the new SFD bearing.

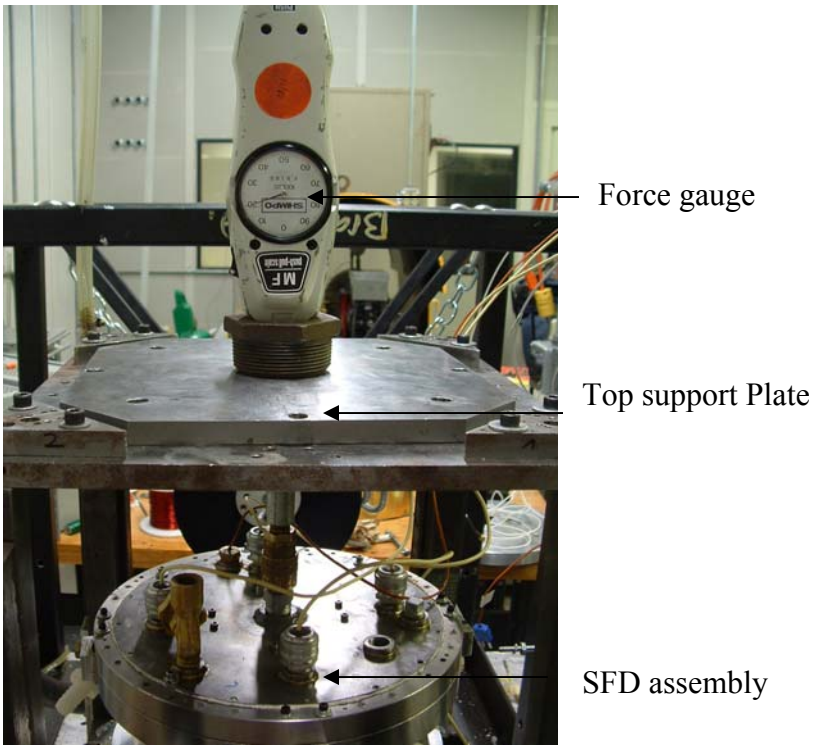

Figure 6 Setup for measuring the weight of SFD assembly.

Static load tests using a force gauge (±0.5 lb) and two eddy current sensors (X_2, Y_2) yield two stiffness parameters (K_{sx}, K_{sy}). No cross-coupled effects were observed during static loading of the bearing assembly.

Figures 7 and 8 show the bearing deflections in the X and Y directions due to a force exerted in the same direction, respectively. Each data point represents an average of a set of three static load tests. The results follow a linear tendency along the entire range of loads exerted on the SFD assembly (-10 to 10 lb). Thus, a constant stiffness coefficient in each direction (X and Y) is appropriate to characterize the rigidity of the four rods arrangement.

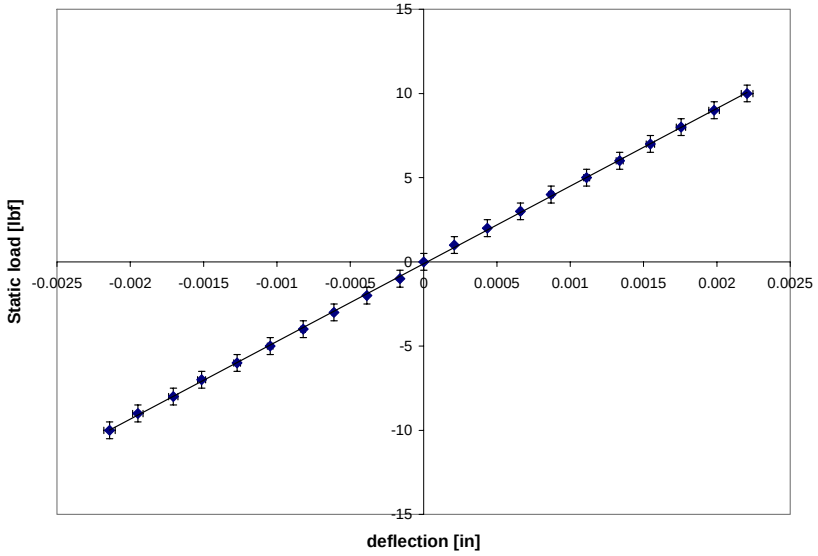

Figure 7 Bearing deflection vs. applied load in the *X* direction due to a force applied in the *X* direction. (U_F: 0.5 lb)

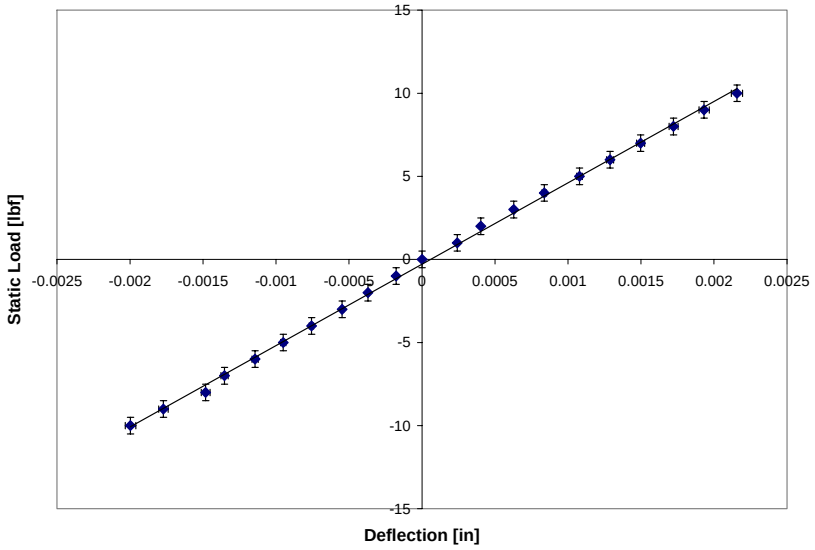

Figure 8 Bearing deflection vs. applied load in the *Y* direction due to a load applied in the *Y* direction. (U_F: 0.5 lb)

Table 3 presents the structure stiffnesses in the *X* and *Y* directions. The values are very close (~7% difference), confirming the symmetry of the arrangement. Furthermore, the present stiffness values coincide (within the uncertainty range) with stiffness values (K_{sx} = 4755 lb/in, K_{sy} = 4823 lb/in) of the previous test rig set up (open-end SFD) [12]. This agreement was anticipated, since the current set up comprises the same structural arrangement (same rods in the same location relative to the SFD assembly).

Table 3 Structural stiffness coefficients of bearing support from static tests

	K_{sx}[lb/in]	K_{sy}[lb/in]
Value	4610 (807.3 x10^3 N/m)	4902 (858.5 x10^3 N/m)
Uncertainty	141(24.7 x10^3 N/m) [~3%]	171 (29.9 x10^3 N/m) [~3.5%]
Range[lb]	-10 to 10	-10 to 10
f_n* [Hz]	41.9±0.8	43.2±0.9

*: obtained using the stiffnesses and weight measured from static test

Appendix B describes the uncertainty analysis of the reported results.

Impact load tests

A sets of impact tests performed along the X and Y directions of the SFD assembly stand to identify the structural parameters of the bearing assembly. A second set of tests stand to quantify any change in the structural parameters of SFD assembly after connecting the electromagnetic shakers. Figure 9 depicts a schematic view of the test set up and instrumentation.

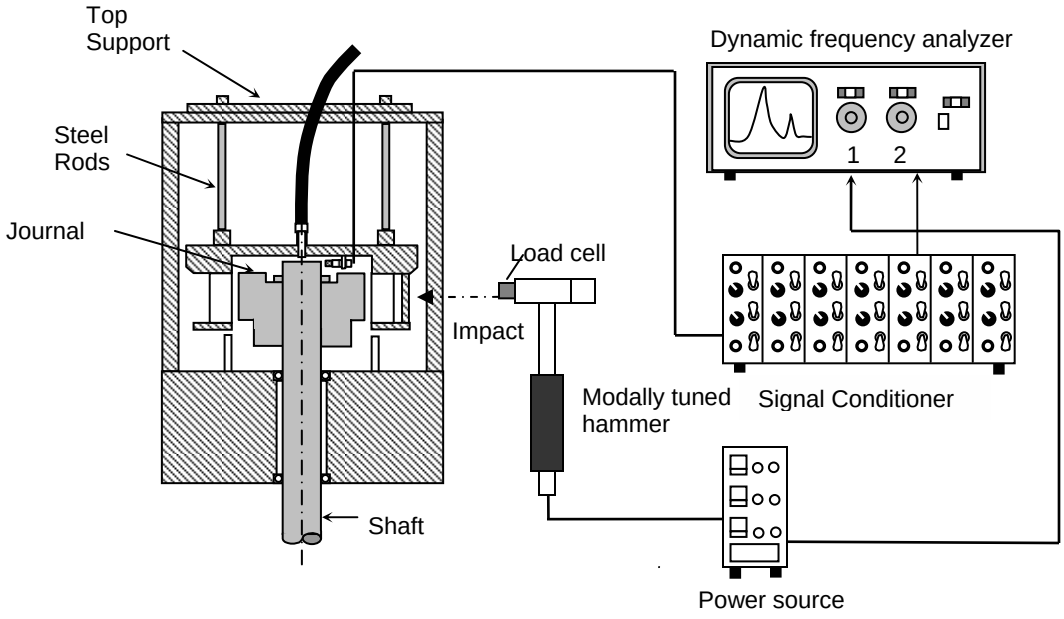

Figure 9 Instrumentation set up for parameter identification via impact tests

The instrumentation for the impact tests consists of

- Two eddy current sensor (X_2, Y_2) (207.1 mV/mil, 208.3 mV/mil)
- Modally tuned impact hammer (load cell 1 mV/lb) and power source
- Signal conditioner (to eliminate DC offset)
- Two channel frequency analyzer

Figure 10 depicts the time trace of a typical impact and displacement registered in the *X* and *Y* directions, respectively. The response of the system is characterized by an oscillatory response with an exponentially decaying amplitude. However, motion in the *Y* direction shows fluctuation like in a beating phenomenon, thus evidencing the closeness of the natural frequencies in the *X* and *Y* directions.

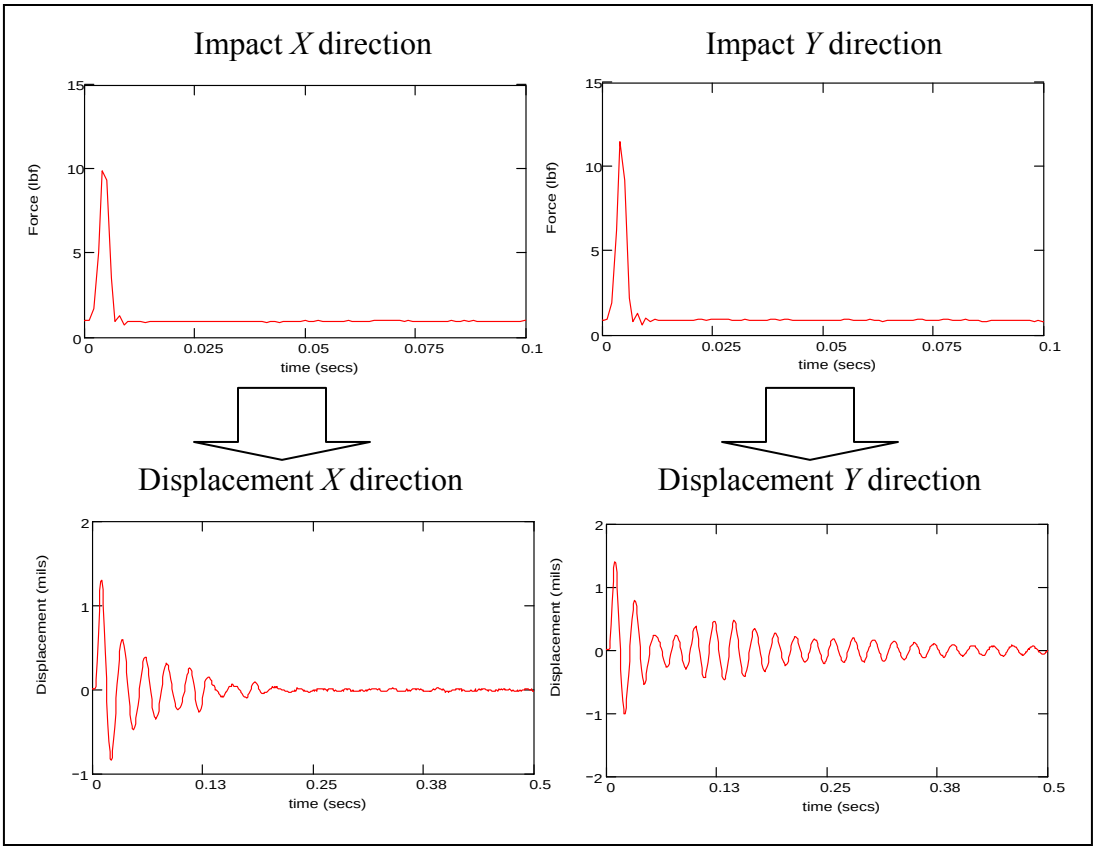

Figure 10 Impact and displacement time traces in the *Y* and *X* directions (Impact load tests)

A curve fit of the system response transfer function (displacement/force), obtained from averaging 10 impacts in each direction (*X* and *Y*), yields the structure stiffness, equivalent mass and damping coefficients of the SFD bearing assembly w/o lubricant. A transfer function of the form

$$H(\omega) = \frac{1}{\left[\left(K_s{}^2 - M\omega^2\right)^2 + (C_s\omega)^2\right]^{1/2}} = \frac{x}{F} \qquad (2)$$

represents the dynamic flexibility of a linear system with viscous damping.

Figures 11 and 12 show the transfer functions of the system in the *X* and *Y* directions with and without the shaker attached to the SFD assembly (top and bottom graphs, respectively). Table 4 presents the results from the impact tests exerted on the bearing assembly. The model transfer has an excellent agreement (±4%) at frequency values close to zero ($f \rightarrow 0$). Recall that the value of the function *H(0)* is the flexibility coefficient (K^{-1}). Therefore, the curve fits yield stiffness coefficients that are in agreement with the stiffness coefficients obtained from the static tests (±2%).

The mass estimated from the static tests (measured weight and static stiffness) is slightly different from the values obtained from the impact tests in the *X* direction (±12%), whereas in the *Y* direction both approaches (impact load and static load tests) render similar values (±3%). The small difference between the results in both impact directions is attributed to the difference on the measuring approach. Impact tests yield values of the equivalent "vibrating mass" corresponding to a specific vibration mode (the fundamental in this case), which can be slightly different from the measured weight. The mass value of the system is then given by the value that better fits both approaches (i.e. 27 lb in *X* direction and 25 lb in *Y* direction).

Regarding the viscous damping coefficients, the transfer functions show very little damping on the order of 8 % or less which is typical of steel structures [13]. These damping coefficients (C_{sx}, C_{sy}) are also very small in comparison with the viscous damping coefficients arising from the SFD oil film.

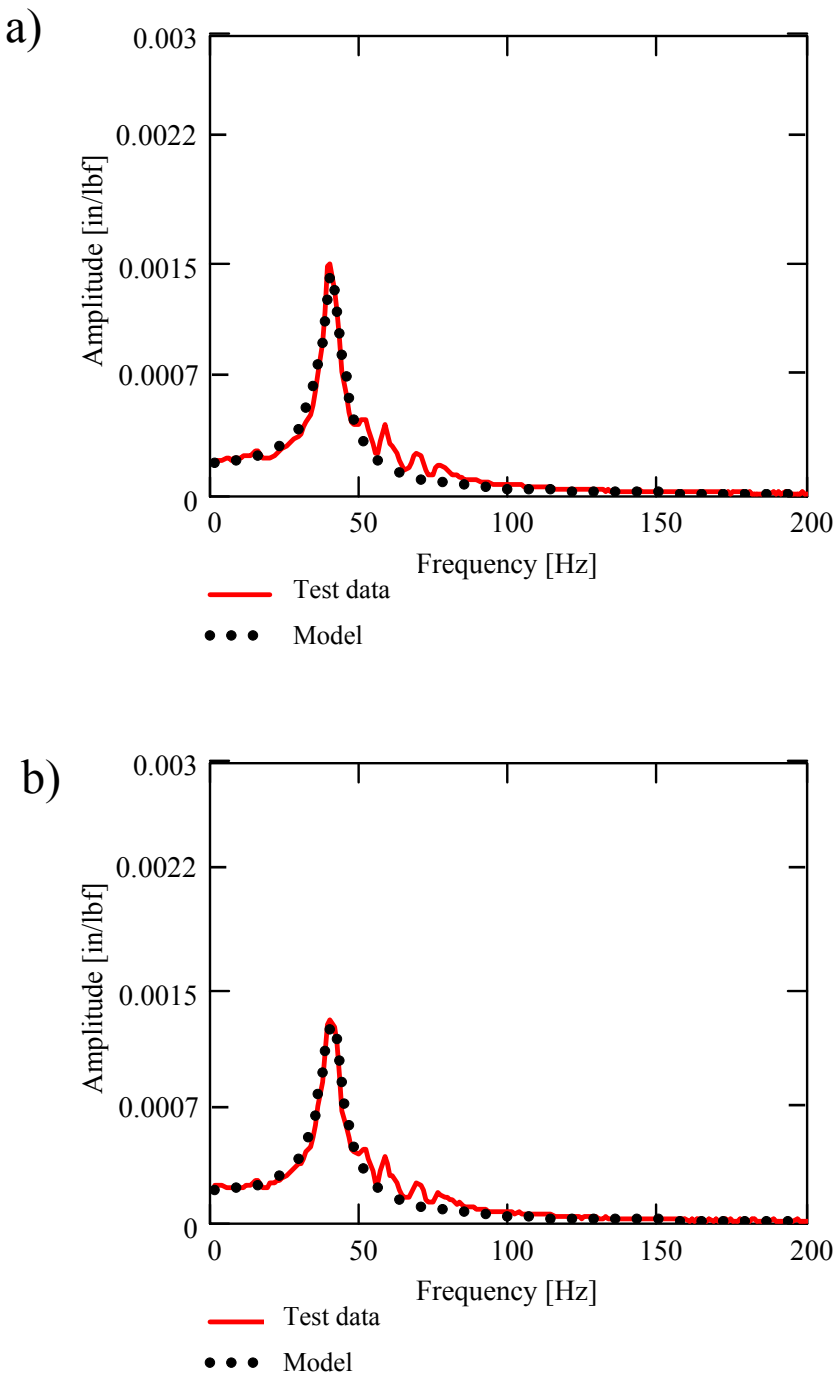

Figure 11 Transfer function and model fit in the *X* direction for (a) bearing assembly and (b) bearing assembly + shakers.

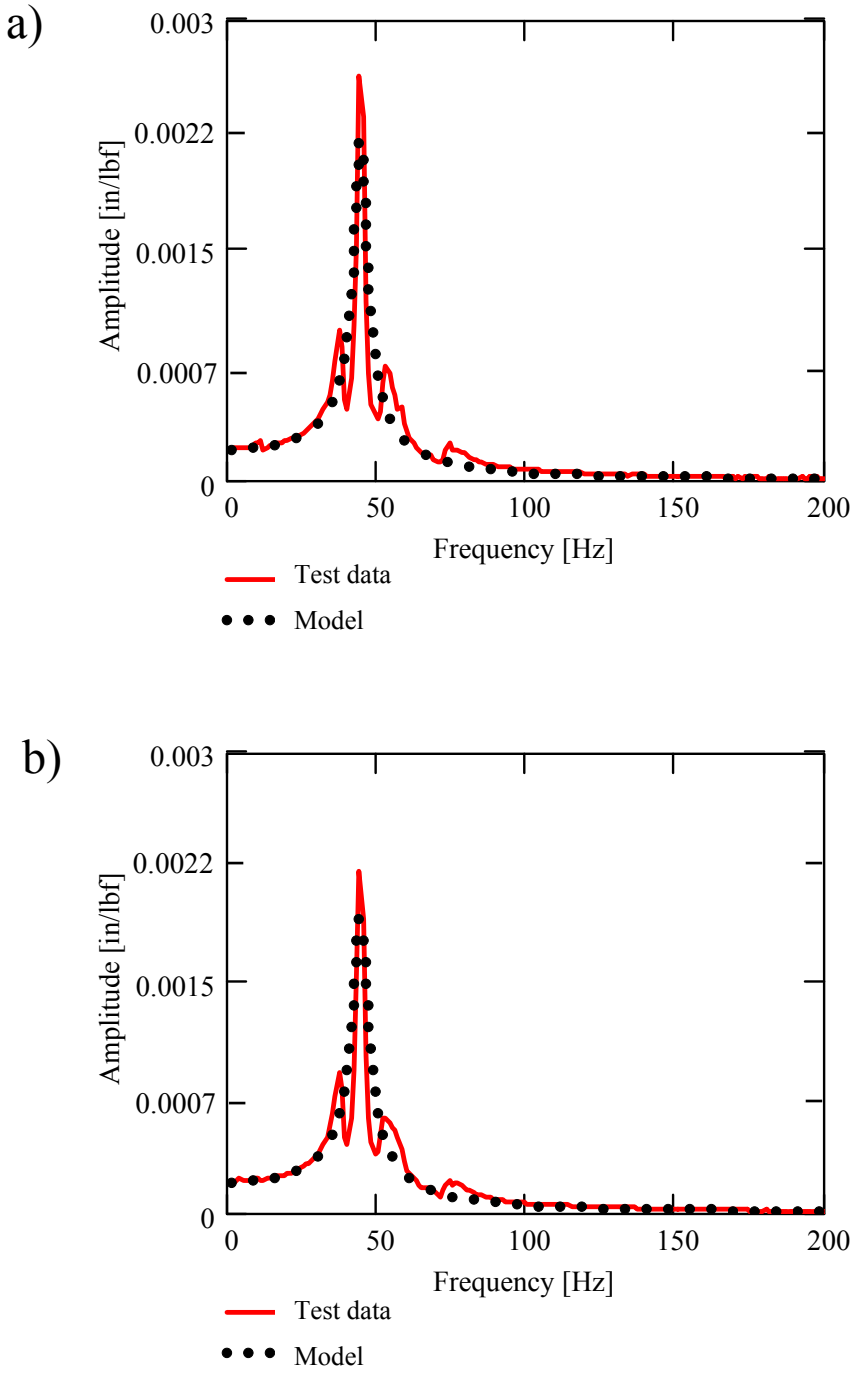

Figure 12 Transfer function and model fit in the *Y* direction for (a) bearing assembly and (b) bearing assembly + shakers.

Table 4 Identified parameters from impact tests exerted on SFD test section (with and w/o shaker attached to the assembly)

		w/o shaker		with shaker	
	Parameters	*X*	*Y*	*X*	*Y*
US	Stiffness K_s [lb/in]	4687 (±234)	4988 (±249)	4792 (±240)	5101 (±255)
	Mass *M* [lb]	28 (±1.1)	25 (±0.9)	28 (±1.1)	26 (±1.0)
	Damping *C* [lb.s/in]	2.87	1.63	3.20	2.125
SI	Stiffness K_s [N/m]x10^3	8.21 (±0.49)	8.73 (±0.44)	8.39 (±0.42)	8.93 (±0.45)
	Mass *M* [Kg]	12.7 (±0.5)	11.3 (±0.4)	12.7 (±0.5)	11.9 (±0.4)
	Damping *C* [N.s/m]	502	285	560	372
	Damping ratio ζ	0.078	0.045	0.085	0.052
	Natural Frequency f_n[Hz]	40 ±1	44 ±1	40 ±1	44 ±1
	R^2	0.97	0.89	0.97	0.89

Range [Hz]: 1- 100.

Notice that the stiffness and equivalent mass coefficients in the *X* and *Y* directions do not show a significant variation after connecting the shakers to the system (~2%). On the other hand, the damping coefficients increased slightly, which still makes the damping ratio of the system less than 9% (i.e. very low). The results indicate that attaching the shakers to the SFD test housing does not have a notorious influence on its structural parameters.

Figure 13 depicts the coherence for the four impact tests, showing that the parameters identified from the impact tests are valid for the frequency range from one Hz to 100 Hz.

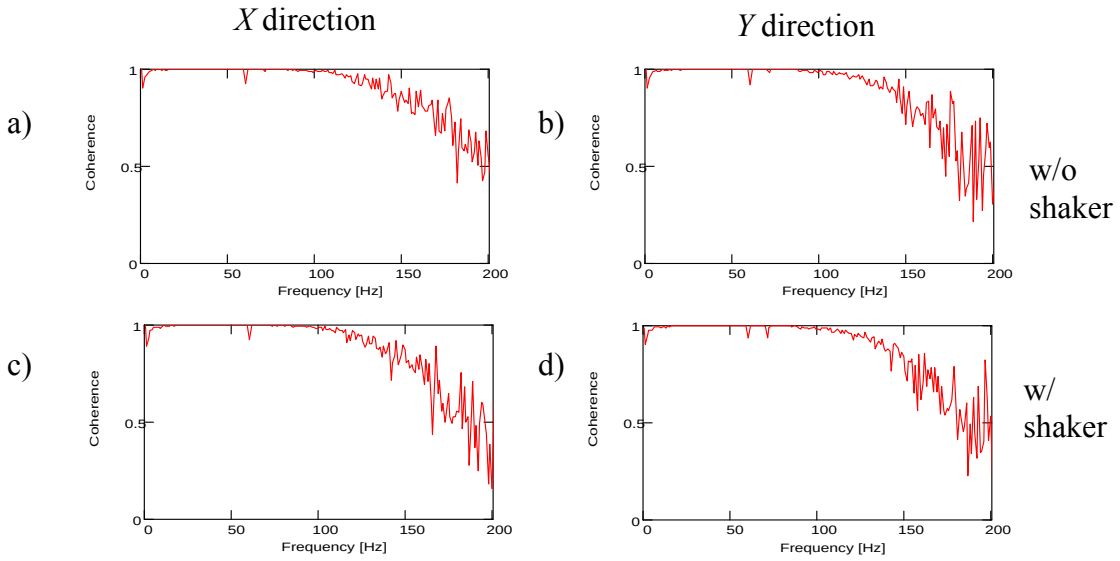

Figure 13 Coherence from 10 impacts in the (a and b) *X* and *Y* direction w/o shaker, (c and d) *X* and *Y* direction w/o shaker, respectively.

Planned testing and parameter identification method

The experiments for identification of SFD coefficients will comprise single frequency (periodic) loads with different magnitudes, and multi-frequency excitation with constant magnitude force. For the first case, the electromagnetic shakers will excite the SFD assembly along directions (*X,Y*) to produce elliptical bearing motions. This excitation will be at a constant frequency and for different orbit amplitudes (i.e. different force magnitudes). The excitation frequencies will be selected (40, 50, 60 Hz) around the "dry" system natural frequency (~40 Hz) to make more apparent the effect of squeeze film damping on the bearing force response.

For the multi-frequency tests, a sweep sine function will drive the electromagnetic shakers, over a frequency range from 5 to 100 Hz. For both cases, the tests will be conducted with various lubricant temperatures (max 120 ^{0}F) and supply pressures (up to 20 psig).

The identification procedure for estimation of system parameters follows a method in the frequency domain described in [14]. The equations of motion for the test bearing section are

$$\begin{bmatrix} M+M_f & 0 \\ 0 & M+M_f \end{bmatrix} \begin{Bmatrix} \ddot{x} \\ \ddot{y} \end{Bmatrix} + \begin{bmatrix} K_{sx} & 0 \\ 0 & K_{sy} \end{bmatrix} \begin{Bmatrix} x \\ y \end{Bmatrix} = \begin{Bmatrix} F_x \\ F_y \end{Bmatrix} - \begin{Bmatrix} F_x \\ F_y \end{Bmatrix}_{Bearing} \tag{3}$$

The SFD bearing reaction forces are defined by the linearized description

$$\begin{Bmatrix} F_x \\ F_y \end{Bmatrix}_{Bearing} = \begin{bmatrix} C_{xx} & C_{xy} \\ C_{yx} & C_{yy} \end{bmatrix} \begin{Bmatrix} \dot{x} \\ \dot{y} \end{Bmatrix} + \begin{bmatrix} D_{xx} & D_{xy} \\ D_{yx} & D_{yy} \end{bmatrix} \begin{Bmatrix} \ddot{x} \\ \ddot{y} \end{Bmatrix} \tag{4}$$

where $\{C_{\alpha\beta}\}_{\alpha\beta=x,y}$ $\{D_{\alpha\beta}\}_{\alpha\beta=x,y}$ are the damping and inertia force coefficients, respectively. The term M_f represents the mass of fluid enclosed in the plenum above the fluid film land section and in the recirculation annulus. Recall that a squeeze film damper does <u>not</u> generate stiffness coefficients. The analysis also disregards the "dry" damping coefficients $(C_s)_{x,y}$ since their magnitudes are a minute fraction (see previous section) of the (expected) squeeze film damping coefficients.

In the frequency domain the motion of the system can be described as

$$\left[-\omega^2 \boldsymbol{M} + i\omega \boldsymbol{C} + \boldsymbol{K}\right] Z_{(\omega)} = \underline{H}_{(\omega)} F_{(\omega)} \tag{5}$$

where

$$\boldsymbol{M} = \begin{bmatrix} M + M_f + D_{xx} & 0 \\ 0 & M + M_f + D_{yy} \end{bmatrix},\ \boldsymbol{K} = \begin{bmatrix} K_{sx} & 0 \\ 0 & K_{sy} \end{bmatrix},\ \boldsymbol{C} = \begin{bmatrix} C_{xx} & C_{xy} \\ C_{yx} & C_{yy} \end{bmatrix}, \tag{6}$$

and $Z_{(\omega)}, F_{(\omega)}$ are the discrete Fourier Transform (DFT) of time varying displacements and forces, respectively. In particular, a periodic forcing function can be represented as

$$\begin{aligned} F_x(t) &= F_{xc}\cos(\omega t) + F_{xs}\sin(\omega t) = \left(F_{xc} - i\,F_{xs}\right) e^{i\omega t} = \bar{F}_x\, e^{i\omega t} \\ F_y(t) &= F_{yc}\cos(\omega t) + F_{ys}\sin(\omega t) = \left(F_{yc} - i\,F_{ys}\right) e^{i\omega t} = \bar{F}_y\, e^{i\omega t} \end{aligned} \tag{7}$$

Subsequently, the bearing displacement and accelerations are also periodic with identical frequency (ω), and can be expressed as

$$Z_{(\omega)} = \begin{Bmatrix} x \\ y \end{Bmatrix} = \begin{Bmatrix} x_c - i\,x_s \\ y_c - i\,y_s \end{Bmatrix} e^{i\omega t} = \begin{Bmatrix} \bar{x} \\ \bar{y} \end{Bmatrix} e^{i\omega t};\ \begin{Bmatrix} \ddot{x} \\ \ddot{y} \end{Bmatrix} = \begin{Bmatrix} \bar{a}_x \\ \bar{a}_y \end{Bmatrix} e^{i\omega t} \tag{8}$$

The impedance matrix ($\underline{H}_{(\omega)}$) includes four coefficients, which are complex algebraic functions of the excitation frequency (ω). Equation (5) provides just two equations. Thus, two linearly independent excitations become mandatory to find the four SFD force coefficients. For the single frequency tests, the SFD force coefficients are determined from

$$\underline{H}_{(\omega)} = [F^1{}_{(\omega)} \vdots F^2{}_{(\omega)}][Z^1{}_{(\omega)} \vdots Z^2{}_{(\omega)}]^{-1} \tag{9}$$

Rearranging equation (8), locating the know parameters in one side of the equation and expressing the result in terms of the bearing coefficients yields [3]

$$\begin{bmatrix} C_{xx}-\omega D_{xx} & i\omega C_{xy}-\omega D_{xy} \\ C_{yx}-\omega D_{yx} & i\omega C_{yy}-\omega D_{yy} \end{bmatrix} \begin{Bmatrix} \overline{x} \\ \overline{y} \end{Bmatrix} = -i\omega \begin{bmatrix} \overline{P}_x^{(1)} & \overline{P}_x^{(2)} \\ \overline{P}_y^{(1)} & \overline{P}_y^{(2)} \end{bmatrix} \begin{bmatrix} \overline{x}^{(1)} & \overline{x}^{(2)} \\ \overline{y}^{(1)} & \overline{y}^{(2)} \end{bmatrix} \tag{10}$$

with

$$\begin{Bmatrix} \overline{P}_x \\ \overline{P}_y \end{Bmatrix} = \begin{Bmatrix} \overline{F}_x \\ \overline{F}_y \end{Bmatrix} - \begin{bmatrix} M+M_f & 0 \\ 0 & M+M_f \end{bmatrix} \begin{Bmatrix} \overline{a}_x \\ \overline{a}_y \end{Bmatrix} - \begin{bmatrix} K_{sx} & 0 \\ 0 & K_{sy} \end{bmatrix} \begin{Bmatrix} \overline{x} \\ \overline{y} \end{Bmatrix} \tag{11}$$

The vector $\{\overline{P}_x, \overline{P}_y\}^T$ comprises known parameters measured during experimentation (forces, bearing displacements and accelerations), and parameters of the "dry" system identified earlier (mass and stiffness). Equation (9) is complex in character, thus allowing direct evaluation of the SFD damping and inertia force coefficients at the excitation frequency (ω).

For the multi-frequency tests, in particular sweep sine forcing function, the application of the DTF to the measured forces and displacements yields discrete algebraic equations in the frequency domain. Thus, from equation (8), the k^{th} impedance matrix is given by:

$$\underline{H}^k = [F^1_{(\omega_k)} \vdots F^2_{(\omega_k)}][Z^1_{(\omega_k)} \vdots Z^2_{(\omega_k)}]^{-1} \tag{12}$$

The SFD force parameters will be determined using the Instrumental Variable Filter method [14, 5]. Existing software will process the recorded time data (displacements, acceleration, forces), transform the data into the frequency domain, and build the system of equations to obtain the coefficients using the IVF method.

A parameter identification of the sealed end SFD damper will follow after the parameter characterization of the open end configuration. A priori, the parameter identification for the sealed configuration will follow the same procedure described above. However, dry-friction forces or Coulomb-like damping arising from the sliding surfaces (end seal) may have a significant influence on the SFD forced response. In particular, if large portions of the surfaces in contact remain dry or scarcely lubricated, the presence of dry friction can lead to a highly non-linear system (multiple frequency response) not amenable for a linear analysis. If that is the case, a procedure described by San Andrés and Aguilar [15], based on Rice and Fitzpatrick [16] frequency domain identification method, will be implemented to identify the system parameters (viscous and dry friction).

Closure

The identification of the structural parameters of the test bearing section, through static and impact tests, rendered consistent values of stiffness and effective mass (K_{sx} ~ 4600 [lbf/in], K_{sy} ~ 4900 [lbf/in], M_{xx} ~ 27 lbm, M_{yy} ~ 25 lbm). An uncertainty analysis (Appendix B) provides a "confidence" interval of the results. The damping coefficients are considerably smaller (ζ~8%) than those expected from the test section under operation conditions (i.e. with lubricant running through the SFD land).

The planned experimentation and parameter identification method to determine SFD force coefficients method were described. A method for identification of non-linear system parameters is also available in case the response of the system is influenced by dry friction effects arising from the contact end seal (sliding surfaces).

References

[1] Rodriguez, L., Diaz, S., and San Andrés, L., 2000, "Sine Sweep load Versus Impact Excitations and their Influence on the Identification of Damping in a Bubbly Oil Squeeze Film Damper," TRC report, TRC-SFD-3-00, May.

[2] Zeidan, F.Y., San Andrés, L., and Vance, J. M., 1996, "Design and Application of Squeeze Film Dampers in Rotating Machinery," Proceedings of the 25th Turbomachinery Simposium, Houston, TX, pp.169-188.

[3] Diaz, S., and San Andrés, L., 2000, "Orbit-based Identification of Damping Coefficients of Off-centered Squeeze Film Damper including Support Flexibility," ASME Paper 2000-GT-0394.

[4] San Andrés, L., and Diaz, S., 2002, "Flow visualization and Forces from a Squeeze Film Damper with natural air entrapment," ASME Paper 2002-TRIB-81.

[5] Diaz, S., and San Andres, L., 1998, "Design and Application of Squeeze Film Damper operating with a Bubbly lubricant," ASME 98-GT-109.

[6] Diaz, S., and San Andrés, L., 2001, "A Model for Squeeze Film Dampers Operating with Air Entrapment and Validation with experiments," ASME Journal of Tribology, **122**(1), pp. 205-210.

[7] Diaz, S., and San Andrés, L., 2002, "Pressure Measurements and Flow visualization in a Squeeze Film Damper Operating with a Bubbly Mixture," ASME Journal of Tribology, **124**(4), pp. 346-350.

[8] Della Pietra, L., and Adilleta, G., 2002, "The Squeeze Film Damper over Four Decades of Investigations. Part I: Characteristics and Operating Feature," The Shock and Vibration Digest, **34**(1), pp. 3-26.

[9] Levesley, M., and Holmes, R., 1996, "The Effect of Oil Supply and Sealing Arrangements on the Performance of Squeeze-film Dampers: an Experimental Study," Journal of Engineering Tribology: part J, **210**, pp. 221-232.

[10] San Andrés, L., 2002, "Response of a Squeeze Film Damper Under High Dynamic Loading and Identification of Damping and Inertial Coefficients," TRC-SFD-1-02.

[11] San Andrés, L., and Rhode, D., 2003, "Test Force Coefficients for a Sealed Squeeze Film Damper and CFD two-phase flow for predictions of performance," proposal to Honeywell Engines and Systems, Feb.

[12] Romero, F., and Rodriguez, L., 2001, "Identification of Structural Parameters in Vertical Test Rig," Tribology Group, Internal Progress Report, December.

[13] Vance, J. M., 1988, *Rotordynamics of Turbomachinery,* JOHN WILEY & SONS, New York.

[14] Diaz, S., and San Andrés, L., "A Method for Identification of Bearing Force Coefficients and Its Application to a Squeeze Film Damper with a Bubbly Lubricant," STLE Tribology Transactions, Vol. 42 (4), pp. 739-746, 1999.

[15] Fritzen, C., 1985, " Identification of Mass, Damping and Stiffness Matrices of Mechanical Systems," ASME paper 85-DET-91

[16] San Andrés, L., and Aguilar, R., 2000, "Leakage and Dynamic Response of a Hybrid Brush Seal-Gas Damper Seal," TRC-SEAL-3-00.

[17] Rice, H., and Fitzpatrick, J., 1991, " A Procedure for the Identification of Linear and Non-linear Multi-Degree-of-Freedom Systems," Journal of Sound and Vibrations, Vol. 113, pp.132-140.

[18] Coleman, H. W., and Steele, G. W., 1988, *Experimentation and Uncertainty Analysis for Engineers,* JOHN WILEY & SONS, New York.

Appendix A. Calibration of eddy current sensors

This section describes the results and procedure followed for calibrating the eddy current sensors employed in the identification of the test rig structural parameters (static tests).

The calibration of the eddy current sensors was performed in situ (i.e. eddy current sensors attached to the rig). Two dial gauge (± 0.0001) with magnetic bases, located in the *X* and *Y* direction, made it possible to measure the actual displacement of the bearing housing.

The calibration consisted of pushing and pulling the bearing housing while measuring the output voltage of the eddy current sensors every 1 mil (measured with the dial gauge). Table 1 presents the gain of the eddy current sensors estimated from a linear regression of the calibration results shown in Figure A1.

Table A1 Eddy current sensors gain estimated from calibration tests.

	X_1	X_2	Y_1	Y_2
Gain[mV/mils]	217.2	207.1	211.3	208.5
R^2	0.9964	0.9967	0.9976	0.9988
Range[volts] ~	-9.3 to-11.2	-7.4 to-9.2	-8 to -6.1	-3.6 to -5.5
Uncertainty	4%	2%	4%	2%
Serial #	H-108912	H-108877	H-108913	H-108914

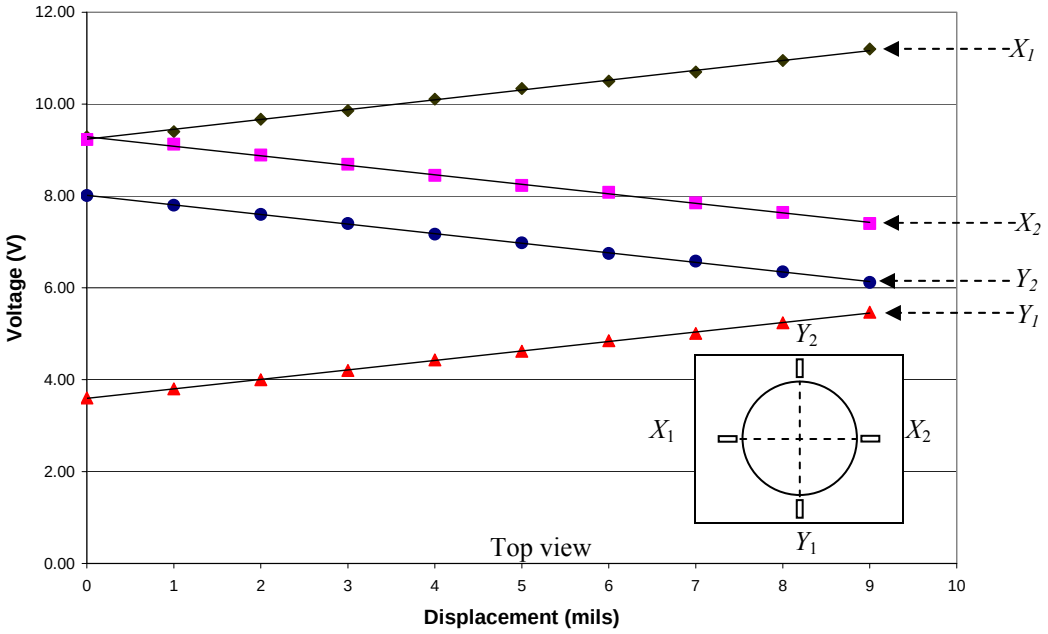

Figure E1 Displacement of SFD bearing vs. Voltage output of eddy current sensors. (Calibration test)

Appendix B. Uncertainty analysis of test data

This section is dedicated to asses the uncertainty associated with the results reported in previous sections. The analysis contemplates the estimation of the error of each individual measurement, as well as the error propagation associated with parameters that are function of other variables.

Eddy current sensor calibration

The calibration of the proximity sensor (Appendix A) included readings from a displacement gauge ($U_d = \pm 0.0001$") and a voltmeter ($U_v = \pm\ 0.001\ V$). The uncertainty at each point is normally given by the precision and bias error of each instrument. However, for this calibration process, the uncertainty of each point (U_d, U_v) does not include the bias error of each instrument. Recall that the bias error is the fixed, systematic, or constant component of total error [17]. Thus, the calculation of the proximity sensor gains is not affected by the bias error, considering that the calculation of such gain is based on the relative value between each measurement (i.e. slope). On the other hand, the standard error of an estimate (*SEE*) can be used to obtain the goodness of the (least-squares) line that best fits the collection of pairs (voltage, displacement). That is, the *SEE*, given in equation (B.1) below, represents the deviation of the curve fit ($y=ax+b$) from the data set. The term "*N-2*" in the denominator arises from the two degrees of freedom lost from the set of N data pairs (X_i, Y_i) when determining the curve constants, a and b (slope and axis intersection) [17].

$$SEE = \left(\frac{\sum_{i=1}^{N} \left[Y_i - (aXi + b) \right]^2}{N - 2} \right)^{1/2} \tag{B.1}$$

The proximity sensor gain, given by the slope (a) of the curve fit, also follows the relationship

$$G = \frac{\Delta D}{\Delta V_{fit}} \tag{B.2}$$

with ΔD as the displacement variation and ΔV_{fit} as the voltage variation given by the linear fit.

The general equation used for calculating the uncertainty of parameters that are calculated from direct relations (i.e. $r=f(x_1,x_2,..x_n)$) is defined as [17]

$$U_r = \sqrt{\left(\frac{\partial r}{\partial x_1}U_{x_1}\right)^2 + \left(\frac{\partial r}{\partial x_2}U_{x_2}\right)^2 + ... + \left(\frac{\partial r}{\partial x_n}U_{x_n}\right)^2} \tag{B.3}$$

Then, from Equation B.3 the uncertainty of expression B.2 is

$$\left(\frac{U_G}{G}\right)^2 = \left(\frac{\partial G}{\partial D}\frac{U_D}{G}\right)^2 + \left(\frac{\partial G}{\partial V_{fit}}\frac{U_{V_{fit}}}{G}\right)^2 = \left(\frac{1}{\Delta D}U_D\right)^2 + \left(\frac{1}{\Delta V_{fit}}U_{V_{fit}}\right)^2 \tag{B.4}$$

where ΔD and ΔV_{fit} are given by the range of experimental values and $U_{V_{fit}}$ is calculated combining the voltmeter uncertainty (U_v) and the uncertainty of the curve fit given by the B.1 as

$$U_{V_{fit}} = \sqrt{\left(U_{fit}\right)^2 + \left(U_V\right)^2} \tag{B.5}$$

Parameter Identification

Static test

The procedure to estimate uncertainty of the stiffness resulting from static test is similar to the one followed in the calibration of the proximity sensor. In this case, since each data pair (displacement, force) is the average from three different tests, the uncertainty of each point (in the displacement axis) of the force vs. displacement data collection is given by the combination of the instrument uncertainty (i.e. voltimeter) and the error incurred from averaging the three test, which is given by

$$U_{avg} = tS_{\bar{x}} \quad \text{t=4.303}$$

$$S_{\bar{x}} = S_x / \sqrt{N} \;\; ; \qquad S_x = \left[\frac{1}{N-1}\sum_{i=0}^{N}\left(X_i - \bar{X}\right)^2\right]^{1/2} \tag{B.6}$$

where $S_{\bar{x}}$ is the precision index of the mean value, S_x is the precision index; and, $\bar{X}$ and X_i represent the mean of the sample array and the individual samples, respectively. And t

is coefficient for 2 degrees of freedom (N-1) and a 95% confidence interval for a t-distribution of data points [17].

Subsequently, the uncertainty of the linear fit is given by B.1 and the uncertainty associated with the slope (stiffness coefficient) is defined as

$$\left(\frac{U_K}{K}\right)^2 = \left(\frac{1}{\Delta F}U_F\right)^2 + \left(\frac{1}{\Delta D_{fit}}U_{D_{fit}}\right)^2 + \left(\frac{1}{G}U_G\right)^2 \tag{B.7}$$

where

$$K = \frac{G}{V}F \tag{B.8}$$

Impact tests

For this case the uncertainty in the stiffness and mass coefficients is given by the uncertainty associated with the measurements of displacement and force (i.e. instrumentation uncertainty) and the error from the transfer function fit.

$$H(\omega) = \frac{1}{\left[\left(K^2 - M\omega^2\right)^2 + (C\omega)^2\right]^{1/2}} \tag{B.9}$$

This assumption is valid for stiffness and mass coefficient only, regarding that the curve fit matches the measured flexibility (i.e. displacement/ force) at $\omega \rightarrow 0$ (±4%), and that the stiffness and the mass given by the numerical fit follow from the expressions

$$H_{fit}(0) = \frac{1}{K}, \quad M = \frac{K}{\omega_n{}^2} \tag{B.10}$$

where the uncertainty of the natural frequency ω_n is given by the window resolution used in the dynamic frequency analyzer (400 Hz/400 lines= ± 1Hz resolution).

Therefore, the uncertainties of the stiffness and mass are

$$\frac{U_K}{K} = \frac{U_{H_{fit}}}{H(0)}, \quad \left(\frac{U_M}{M}\right)^2 = \left(\frac{U_K}{K}\right)^2 + \left(\frac{2U_K}{\omega_n}\right)^2 \tag{B.11}$$

where

$$\left(\frac{U_{H_{fit}}}{H_{fit}}\right)^2 = \left(\frac{U_F}{F}\right)^2 + \left(\frac{U_D}{D}\right)^2 + \left(1 - \frac{H}{H_{fit}}\right)^2$$

and

$\left(\frac{U_F}{F}\right) = 0.01$ (1% linearity), $\left(\frac{U_D}{D}\right)^2 = \left(\frac{0.0008}{.03019}\right) = 7.84x10^{-4}$